Original

Evaluation of Particle-Emission Cross Sections and Energy Spectra for ^{51}V

Takaaki OHSAWA and Toshikazu SHIBATA

(Received : September 30. 1989)

With the aim of providing data necessary for estimation of induced radioactivity and gas-production rate in the first wall of a fusion reactor, an attempt was made to evaluate the particle-emission cross sections and energy spectra of the emitted particles for vanadium-51, one of the candidate materials. The evaluation was based mainly on the calculations in the framework of the pre-equilibrium model of nuclear reactions. The major part of the calculations were done using simplified version of the model. For comparison purpose, calculations were done also with a more sophisticated code of the model. Possible reasons of the observed differences between the two results were discussed.

KEYWORDS

Fusion reactor, structural material, V-51, pre-equilibrium process, particle-emission cross section, energy spectrum.

I. Introduction

Intreaction of fast neutrons with structural materials of a fusion reactor leads to production of radioactive nuclides, which make it difficult for a man to approach the device for maintenance and repairs. Particle-emission reactions, such as (n, p), (n, α), (n, d), (n, xp), (n, xα), *etc.*, give rise to gas-production in materials, which causes blistering and flaking of the first wall. It is therefore necessary that exact data should be known for the reaction cross sections and energy spectra of the emitted particles in order to evaluate the fitness of materials as fusion reactor structural materials.

It is well known that at around 14 MeV the pre-equilibrium (abbreviated as PE hereafter) process plays an important role in particle-emission reactions. Since full PE plus equilibrium calculation with angular momentum conservation requires a lot of input data and long computing time, it would be useful if a simplified version of the model can be used without serious error in results. In the present study, use was made of a simplified PE code PEGASUS[1] which runs on a personal computer. In parallel to this, calculations were also made using the full PE code TNG[2] for comparison purpose.

Among many candidates of fusion reactor structural materials, choice was made of

vanadium-51, because fair amount of measured data with good accuracy were available and this nuclide was free from strong peculiarities such as shell effects. These are conditions favorable for the validity of the simplified PE code.

Section II describes the models and input data used in the present work. The results of the calculations, including sensitivity analysis to input physical quantities, the effects of the PE process and comparison of results from simplified and full PE calcualtions, are shown in section III. Some discussions and comments on the results are given in section IV.

II. The Models

1. Simplified PE Model

The code PEGASUS[1] is based on the closed-form exciton and multistep evaporation model. This model does not take into account the angular momentum conservation nor the low-lying discrete levels. This simplification may lead to inaccuracies in the calculated cross section near the threshold region, but on the other hand greatly reduce the computing time and the amount of input data. In this code, the first-step particle emission is treated as PE-emission from doorway states followed by evaporation from the compound nucleus, while the second-step process is assumed to be described as simple evaporation with the gamma-competition taken into consideration.

1.1 First-step process

The first-step reaction cross section is given as the sum of PE- and equilibrium contributions:

$$\sigma_{n,x}(E_N,\varepsilon_x)=\sigma^{pre}_{n,x}(E_N,\varepsilon_x)+D(\bar{n},Ec)\sigma^{eq}_{n,x}(E_N,\varepsilon_x) \tag{1}$$

where E_N is the incident neutron energy, ε_x the emitted particle energy, $\sigma^{pre}_{n,x}$ the PE cross section, and $\sigma^{eq}_{n,x}$ the equilibrium cross section. $D(\bar{n},Ec)$ is the depletion factor at the compound-nucleus excitation energy Ec for the equilibrium exciton state (with the exciton number $\bar{n}$) and is given as

$$D(\bar{n},Ec)=\{\sigma_{CN}(E_N)-\sigma^{pre}_{tot}(E_N)\}/\sigma_{CN}(E_N) \tag{2}$$

where σ_{CN} is the compound-formation cross section.

Application of the closed-form exciton model to the PE process and the evaporation model (taking no account of the angular momentum conservation) to the equilibrium process yields the following equations:

$$\sigma^{pre}_{n,x}(E_N,\varepsilon_x)=\sigma_{CN}\cdot\sum_{n=3}^{\bar{n}}W_x(n,Ec,\varepsilon_x)\tau(n,Ec) \tag{3}$$

$$\sigma^{eq}_{n,x}(E_N,\varepsilon_x)=\sigma_{CN}\cdot\frac{\Gamma_x(Ec)}{\sum_y\Gamma_y(Ec)}\cdot\frac{g_x(Ec,\varepsilon_x)}{\Gamma_x(Ec)} \tag{4}$$

where $W_x(n,Ec,\varepsilon_x)$ is the emission rate of a particle x from the n-exciton state, Γ_x the particle-emission width from the compound nucleus, g_x the energy spectrum of the emit-

ted particle from the compound nucleus, and τ the exciton lifetime. These quantities are calculated as described below.

(a) Equilibrium emission

The particle-emission width Γ_x is expressed using the energy spectrum g_x as

$$\Gamma_x(E_C)=\int_0^{E_N-B_x} g_x(E_C,\varepsilon_x)d\varepsilon_x \tag{5}$$

From the principle of detailed balance,

$$g_x(E_C,\varepsilon_x)=C_x\varepsilon_x\sigma_{inv}^{(x)}(\varepsilon_x)\frac{\rho_x(U)}{\rho_C(E_C)} \tag{6}$$

$$C_x=\frac{2s_x+1}{2\pi^2}\cdot\frac{2\mu_x}{\hbar^2}=0.244(2s_x+1)\frac{\mu_x}{m_N} \tag{7}$$

where s_x and μ_x are the spin and reduced mass of the particle x, m_N the neutron mass, $\rho_x(E)$ the level density of the residual nucleus after (n,x) reaction, $\rho_C(E)$ the level density of the compound nucleus, $\sigma_{inv}^{(x)}$ the inverse reaction cross section for incident particle x, B_x the threshold energy of the (n,x) reaction, and $U=E_N-B_x-\varepsilon_x$ the excitation energy of the residual nucleus. The level density formula of Gilbet-Cameron[3] was employed for ρ_x and ρ_C. Using the values of a and T read from the level density file, the code calculates the values of U_x and C_x according to the following equations derived from the condition of smooth junction of Fermi-gas and constant-temperature formulas:

$$x=\frac{1}{2}[aT+\sqrt{(aT)^2-6aT}] \quad (aT\geqq 6) \tag{8}$$

$$x=\sqrt{aU_x}$$

$$C_x=\frac{1}{Texp(\Delta/T)}\cdot\frac{1}{1.447A^{1/3}}\cdot\frac{exp(x)}{x(x-3/2)} \tag{9}$$

(b) Preequilibrium emission

Writing the probability of finding the system in an n-exciton state at time t as $P(n,t)$, the master equation is given by

$$\frac{dP(n,t)}{dt}=\sum_m\lambda_{m\to n}P(m,t)-P(n,t)\{\sum_m\lambda_{n\to m}+W_n\} \tag{10}$$

The lifetime of n-exciton state is defined by

$$\tau(n)=\int_0^m P(n,t)dt \tag{11}$$

Time integration of the master equation gives

$$P(n,\infty)-P(n,0)=\sum_m\lambda_{m\to n}\tau(m)-\tau(n)\{\sum_m\lambda_{n\to m}+W_n\} \tag{12}$$

Using the "never come back" assumption $\lambda_{m\to m+2}\gg\lambda_{m\to m-2}$ and the initial condition $P(n,0)=\delta(n,n_0)$, we obtain from eq. (12) the lifetime in the closed form approximation:

$$\tau(n,Ec)=\frac{D_n}{\lambda_{i\to i+2}+W_i} \tag{13}$$

$$D(n,Ec)=\prod_{m=3}^{n}\frac{\lambda_{m\to m+2}(Ec)}{\lambda_{m\to m+2}(Ec)+W(m,Ec)} \tag{14}$$

The total emission rate $W(n,Ec)$ appearing in the depletion factor eq. (14) is expressed as

$$W(n,Ec)=\sum_x\int W_x(n,Ec,\varepsilon_x)d\varepsilon_x. \tag{15}$$

The transition rates between the doorway states due to two-body interaction are given by

$$\lambda_{n\to n+2}=\frac{2\pi}{\hbar}|M|^2\frac{gc(gcEc)^2}{2(n+1)} \tag{16}$$

$$\lambda_{n\to n-2}=\frac{2\pi}{\hbar}|M|^2\frac{gcph(n-1)}{2} \tag{17}$$

where the matrix element $|M|^2$ for the two-body interaction is given by

$$|M|^2=K/Ac^3Ec \tag{18}$$

where K is the Kalbach constant.[4] The upper limit $\bar{n}$ for the exciton number is determined from the condition $\lambda_{n\to n+2}=\lambda_{n\to n-2}$:

$$\bar{n}=\sqrt{2gcEc} \tag{19}$$

In the actual calculation, comparison was made between the values obtained from the condition $W(n,Ec)\leqq 10^{-3}\cdot\lambda_{n\to n+2}(Ec)$ in eq. (14) and the value given by eq. (19) and the smaller was adopted for the upper limit $\bar{n}$.

The particle-emission probability W_x is expressed as

$$W_x(n,Ec,\varepsilon_x)=\frac{1}{\hbar}C_x\varepsilon_x\sigma^{(x)}{}_{inv}(\varepsilon_x)\cdot\frac{\omega_R^*(U)}{\omega_C(n,Ec)} \tag{20}$$

where the suffix R stands for the residual nucleus. The state density ω is given by the Ericson formula[5]:

$$\omega(p,h,n)=g\cdot\frac{[g(E-\Delta)A_{ph}]^{p+h-1}}{p!h!(p+h-1)!} \tag{21}$$

$$g=(6/\pi^2)a \tag{22}$$

$$A_{ph}=ph-(1/2)[p(p+1)+h(h+1)] \tag{23}$$

If the value of the Pauli correction factor A_{ph} given above is negative, we set $A_{ph}=0$. The exciton state density of the residual nucleus ω_R* is calculated according to the following formulas:

$$\omega_R^*(U)=R_x(p)\omega_R(p-1,h,U) \quad \text{(nuccleon emission)} \tag{24a}$$

$$=\gamma_x\sum_{l,m}F_{l,m}(\varepsilon_x)\omega_R(p-1,h,U) \quad \text{(cluster particle emission)} \tag{24b}$$

where $R_x(p)$ represents the probability of picking up a particle of type x from the p-particle state and was called the combinatorial factor by Cline.[6] If the emitted particle is

a neutron or a proton, the probability is expressed as

$$R_n(p)=\sum_{i=0}^{p-1}(Z/A)^i(N/A)^{p-1-i}[(p-1)!/(p-1-i)!][(p-i)/i!p] \tag{25a}$$

$$R_p(p)=1-R_n(p) \tag{25b}$$

for a neutron and a proton, respectively.

Equation (24b) was proposed by Iwamoto and Harada.[7-9] The cluster formation factor $F_{l,m}$ represents the probabilty of forming an cluster (composite particle) of type x in the surface region of the nucleus by picking up l and m nucleons from levels above and below the Fermi surface, respectively. The values of this factor (normalized so as the sum over possible combinations of l and m be unity) were given in ref. 7. The coefficient γ_x determines the absolute value. In the present calculation, $F_{l,m}$ was represented in a quadratic form as a function of the kinetic energy ε_x^* of the cluster in the nucleus:

$$F_{l,m}(\varepsilon_x^*)=b_0+b_1\varepsilon_x^*+b_2\varepsilon_x^{*2} \tag{26}$$

where the actual energy of the emitted particle ε_x is the sum of the intranuclear kinitic energy and the Q-value of the reaction:

$$\varepsilon_x=\varepsilon_x^*+Q_{n,x} \tag{27}$$

1.2 Second-step reactions

The second-step reactions are treated in the framework of the evaporation model. The double-differential spectrum is defined as

$$\sigma_{n,xy}(E_N,\varepsilon_x,\varepsilon_y)=\sigma_{n,x}(E_N,\varepsilon_x)\cdot\frac{\Gamma_{xy}(E_N,\varepsilon_x)}{\sum_z\Gamma_{xz}(E_N,\varepsilon_x)}\cdot\frac{g_{xy}(E_N,\varepsilon_x,\varepsilon_y)}{\Gamma_{xy}(E_N,\varepsilon_x)} \tag{28}$$

where $\sigma_{n,x}(E_N,\varepsilon_x)$ is the first-step reaction cross section. $\Gamma_{xy}(E_N,\varepsilon_x)$ is the emission width of the particle y from the residual nucleus with excitation energy $U=E_N-B_x-\varepsilon_x$ after emission of a particle x, and is expressed as

$$\Gamma_{xy}(E_N,\varepsilon_x)=\int_0^{E_N-B_x-\varepsilon_x}g_{xy}(E_N,\varepsilon_x,\varepsilon_y)d\varepsilon_x \tag{29}$$

$$\frac{g_{xy}(E_N,\varepsilon_x,\varepsilon_y)}{\Gamma_{xy}(E_N,\varepsilon_x)}\simeq\frac{\varepsilon_y\sigma_{inv}^{(y)}(\varepsilon_y)exp(-\varepsilon_y/T_{xy})}{\int_0^{E_N-B_x-\varepsilon_x}\varepsilon_y\sigma_{inv}^{(y)}(\varepsilon_y)exp(-\varepsilon_y/T_{xy})d\varepsilon_x} \tag{30}$$

The gamma-emission width is approximately given as

$$\Gamma_{xy}(E_N,\varepsilon_x)\simeq\Gamma_\gamma(E=B_n)F_\gamma(z) \tag{31a}$$

$$F_\gamma(z)=1-(1+z+z^2/2!+z^3/3!+z^4/4!)e^{-z} \tag{31b}$$

$$z=(E_N-B_x-\varepsilon_x)/T_x \tag{31c}$$

From eq. (28), the second-step reaction cross section is expressed as follows:

$$\sigma_{n,xy}(E_N,\varepsilon_x,\varepsilon_y)=\iint\sigma_{n,xy}(E_N,\varepsilon_x,\varepsilon_y)d\varepsilon_xd\varepsilon_y$$

$$=\int_0^{E_N-B_{xy}} \sigma_{n,x}(E_N,\varepsilon_x)\frac{\Gamma_{xy}(E_N,\varepsilon_x)}{\sum_z \Gamma_{xz}(E_N,\varepsilon_x)}d\varepsilon_x \tag{32}$$

The emission spectra of the first and second particles are calculated from the following formulas:

$$\sigma^{(1)}_{n,xy}(E_N,\varepsilon_x)=\int_0^{E_N-B_{xy}-\varepsilon_x}\sigma_{n,xy}(E_N,\varepsilon_x,\varepsilon_y)d\varepsilon_y$$

$$=\sigma_{n,x}(E_N,\varepsilon_x)\cdot\frac{\Gamma_{xy}(E_N,\varepsilon_x)}{\sum_z \Gamma_{xz}(E_N,\varepsilon_x)} \tag{33}$$

$$\sigma^{(2)}_{n,xy}(E_N,\varepsilon_x)=\int_0^{E_N-B_{xy}-\varepsilon_y}\sigma_{n,xy}(E_N,\varepsilon_x,\varepsilon_y)d\varepsilon_x$$

$$=\int_0^{E_N-B_{xy}-\varepsilon_y}\sigma^{(1)}_{n,xy}(E_N,\varepsilon_x)\frac{\varepsilon_y\sigma^{(y)}_{inv}(\varepsilon_y)exp(-\varepsilon_y/T_{xy})}{\int_0^{E_N-B_{xy}-\varepsilon_x}\varepsilon_y\sigma^{(y)}_{inv}(\varepsilon_y)exp(-\varepsilon_y/T_{xy})}d\varepsilon_x \tag{34}$$

2. Inverse Cross Sections

Table I. The optical potential parameter sets used for calculation of the inverse cross sections (The potential depths are in MeV, and the nuclear radii and diffusenesses are in fm).

(a) Proton (F.G.Perey [11])		
$V_0 = 53.3-0.50E+27\ (N-Z)/A+0.4Z/A^{1/3}$,	$r_0=1.25$,	$a_0=0.65$
$W_S = 13.5$	$r_S=1.25$,	$a_S=0.47$
$V_{SO} = 7.5$,	$r_{SO}=1.25$,	$a_{SO}=0.47$
	$r_C=1.25$	
(b) Alpha (Huizenga−Igo [12])		
$V_0 = 50.0$,	$r_0=1.17A^{1/3}+1.77$,	$a_0=0.576$
$W_I = 2.5+0.28N\ (N<28)$	$r_I=1.17A^{1/3}+1.77$,	$a_I=0.576$
$= 6.7+0.133N\ (N>29)$		
$V_{SO} = 0.0$,	$r_C=1.17$	
(c) Deuteron (Lohr−Haeberli [13])		
$V_0 = 91.13+2.2\ (Z/A^{1/3})$,	$r_0=1.05$,	$a_0=0.86$
$W_S = 218/A^{2/3}$,	$r_S=1.43$,	$a_S=0.5+0.013A^{2/3}$
$V_{SO} = 7.0$,	$r_{SO}=0.75$,	$a_{SO}=0.5$
	$r_C=1.3$	
(d) Triton (Becchetti−Greenlees [14])		
$V_0 = 16.5-0.17E-6.40\ (N-Z)/A$,	$r_0=1.20$,	$a_0=0.72$
$W_S = 46.0-0.33E-110\ (N-Z)/A$,	$r_S=1.40$,	$a_S=0.84$
$V_{SO} = 2.5$,	$r_{SO}=1.20$,	$a_{SO}=0.72$
	$r_C=1.30$	
(e) He−3 (Becchetti−Greenlees [14])		
$V_0 = 151.9-0.17E+50\ (N-Z)/A$,	$r_0=1.20$,	$a_0=0.72$
$W_S = 41.7-0.33E+44\ (N-Z)/A$,	$r_S=1.40$,	$a_S=0.88$
$V_{SO} = 2.5$,	$r_{SO}=1.20$,	$a_{SO}=0.72$
	$r_C=1.30$	

The cross sections for inverse processes of neutron-induced reactions, such as (p, n), (α, n), (d, n), (t, n), (^{3}He, n), are required in the calculations. These data were calculated using the optical model/Hauser-Feshbach code ELIESE-Ⅲ[10] adopting the optical-model potential (OMP) parameter sets shown in Table Ⅰ.

3. TNG Calculations

With the aim of comparing the results of the simplified and full PE models, TNG calculations were also undertaken. To make the conditions as equal as possible, the same input data were used for both calculations. However, since the TNG code required additional input data such as level scheme and neutron OMP parameters, suitable choice had to be made for these data. In the present calculation, level schemes were taken from *Table of Isotopes*.[15] Three sets of neutron OMP parameters, *i. e.* Wilmore-Hodgson[16], Becchetti-Greenless[17] and that adopted by S. Tanaka[18] in evaluation for JENDL-2, were used for ^{51}V for comparison purpose. The parameters of these potentials are summerized in Table Ⅱ.

Table Ⅱ. The optical potential parameter sets for neutrons used in TNG calculations (The potential depths are in MeV, and the radii and diffuseness are in fm).

(a) Wilmore−Hodgson[16]		
$V_0 = 47.01 - 0.267E - 0.0018E^2$,	$r_0 = 1.322 - (7.6 \cdot 10^{-4})\,A + (4.0 \cdot 10^{-6})\,A^2 - (8.0 \cdot 10^{-9})\,A^3$	
	$a_0 = 0.660$	
$W_S = 9.52 - 0.053E$,	$r_S = 1.266 - (3.7 \cdot 10^{-4})\,A + (2.0 \cdot 10^{-6})\,A^2 - (4.0 \cdot 10^{-9})\,A^3$	
$W_V = 0.0$	$a_S = 0.48$	
(b) Becchetti−Greenlees[17]		
$V_0 = 56.3 - 0.32E - 24.0\,(N-Z)/A$,	$r_0 = 1.17$,	$a_0 = 0.75$
$W_S = 13.0 - 0.25E - 12.0\,(N-Z)/A$,	$r_S = 1.26$,	$a_S = 0.58$
$W_V = 0.22E - 1.56$,	$r_V = 1.26$,	$a_V = 0.58$
$V_{SO} = 6.2$,	$r_{SO} = 1.01$,	$a_{SO} = 0.75$
(C) Tanaka[18] (for ^{51}V)		
$V_0 = 49.50 - 0.33E$,	$r_0 = 1.23$,	$a_S = 0.65$
$W_S = 4.6 + 0.34E$,	$r_S = 1.23$,	$a_S = 0.48$
$W_V = 0.0$,		
$V_{SO} = 7.0$,	$r_{SO} = 1.23$,	$a_{SO} = 0.65$

Ⅲ. Results

1. Energy spectrum of emitted particles

Energy spectra of emitted neutrons for 14-MeV incident neutrons are shown in Fig. 1. In the low energy region, neutrons from (n, 2n) and (n, n′p) reactions are seen to be major contributors, while above 4.5 MeV neutrons from (n, n′) reactions account for almost all the emitted neutrons. Fig. 2 shows the proton and alpha spectra for 14-MeV

incident neutrons. Principal contributor to the proton spectrum is (n, n′ p) reaction in the region $E_p \leqq 3$MeV, (n,pn′) in the region up to 5.5 MeV, and (n, p) above. The alpha spectrum is composed only of (n, α) reaction, and negligible contribution comes from (n, n′ α) or (n, αn′) reactions.

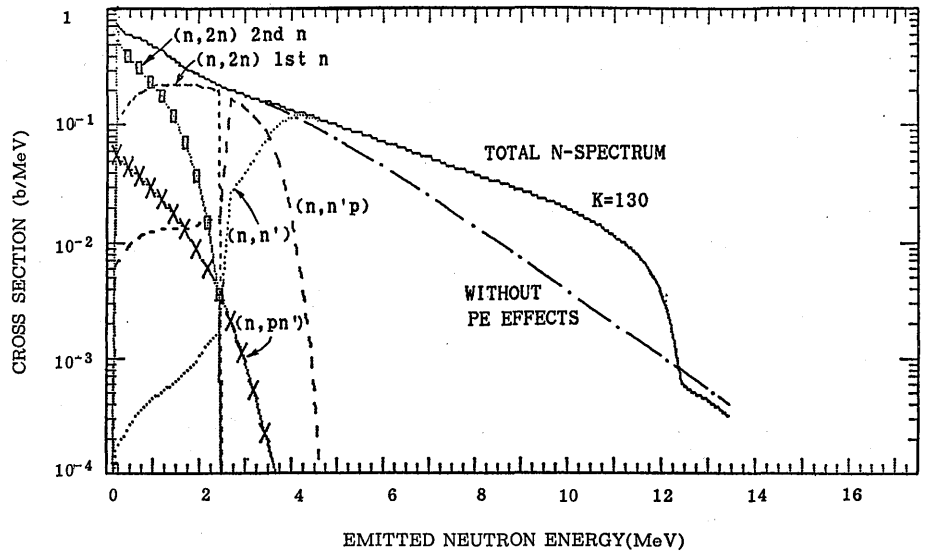

Fig. 1 Spectra of neutrons emitted from ^{51}V bombarded by 14 MeV-neutrons. Total neutron spectrum for the case of absence of PE process is also shown with dash-dot line.

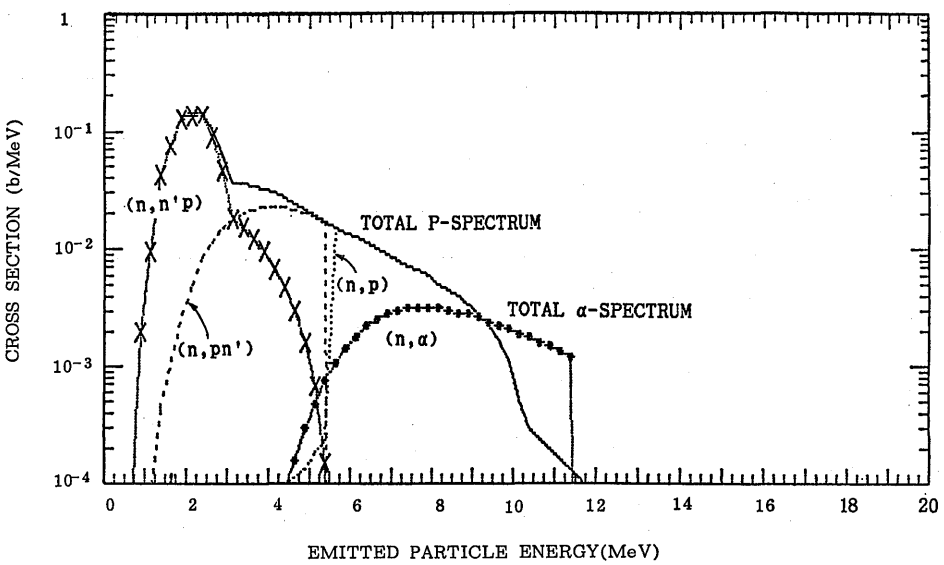

Fig. 2 Spectra of protons and alphas emitted from ^{51}V bombarded by 14 MeV-neutrons.

2. Cross sections

The (n, 2n) cross section is shown in Fig. 3. Present calculation by means of PEGASUS reproduced well the new data of Fréhaut *et al.*[19] TNG calculation with dif-

ferent sets of neutron OMP parameter gave somewhat higher results, the difference due to adopted OMP sets being less than 10%. This group of curves are in agreement with the ENDFD/B-IV evaluation but about 40% higer than the measurement of Fréhaut *et al.*

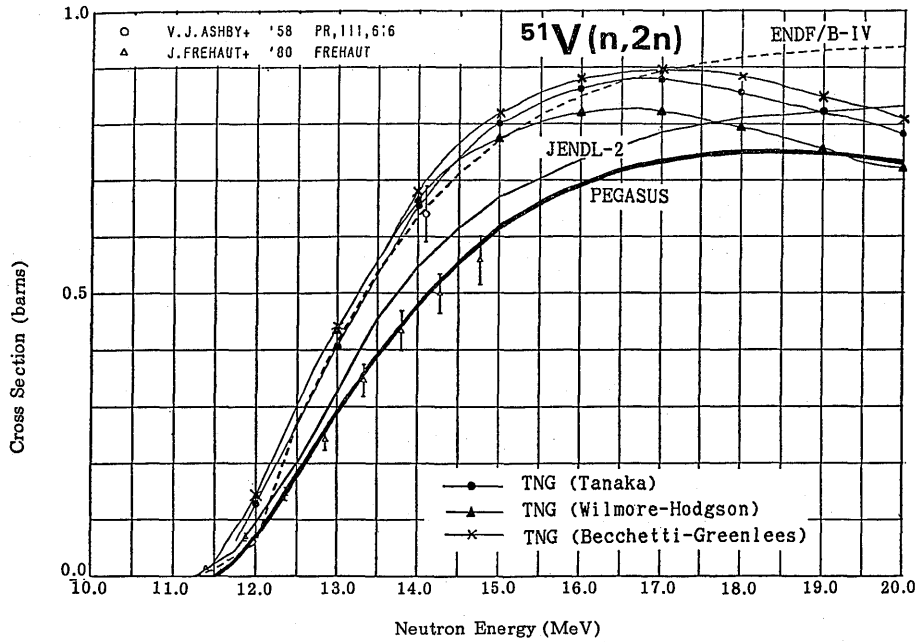

Fig. 3 The (n, 2n) reaction cross section for ^{51}V. The results of PEGASUS- and TNG-calculations (with various OMP parameter sets) are compared. Some experimental data and evaluated values are also shown.

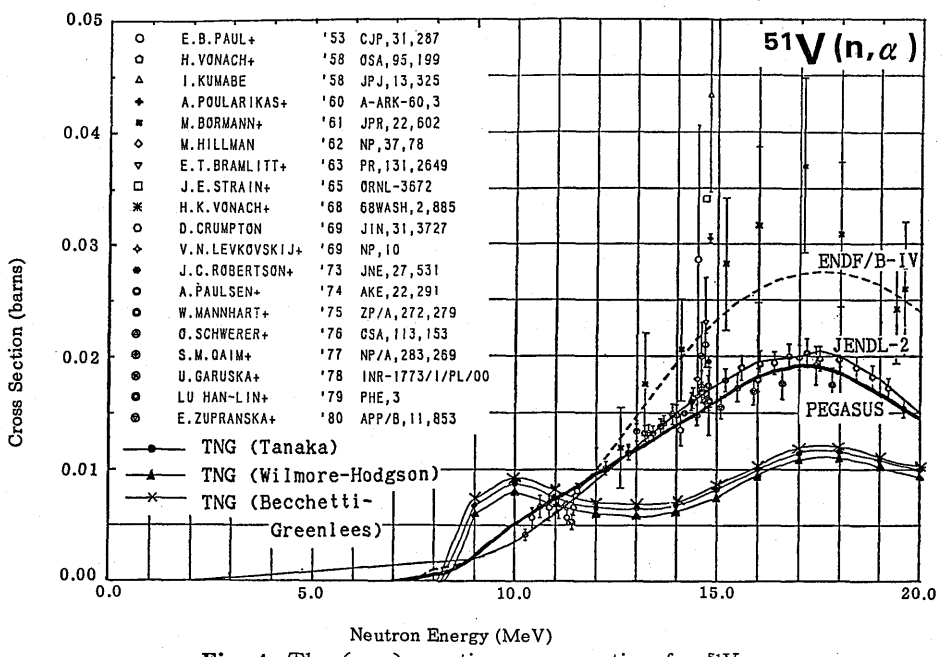

Fig. 4 The (n, α) reaction cross section for ^{51}V.

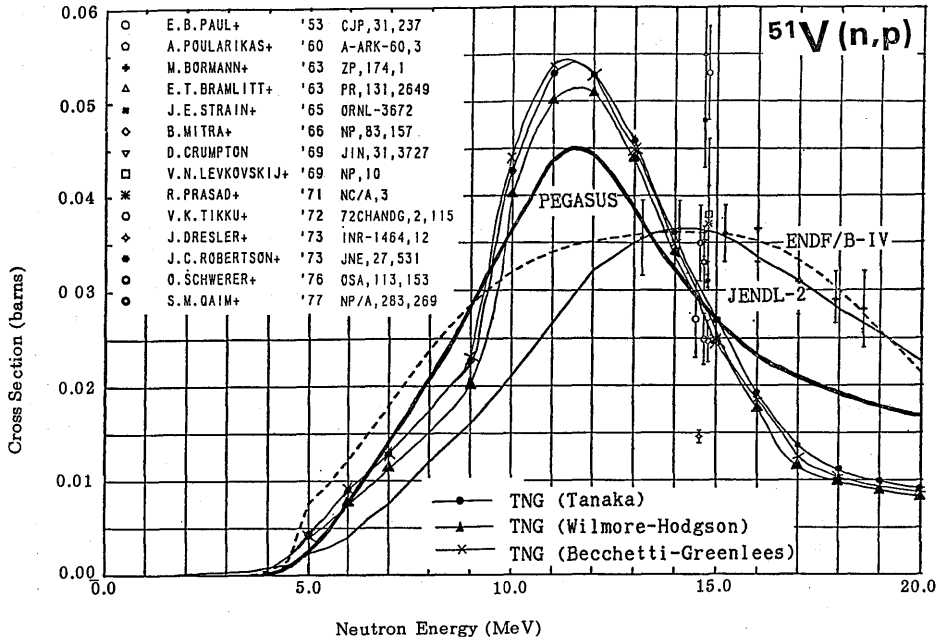

Fig. 5 The (n, p) reaction cross section for ^{51}V.

in the nearthreshold region.

The (n, α) cross section is shown in Fig. 4. There are two groups of measured cross sections; the older measurements (Kumabe,[20] Bormann,[21] Strain,[22] *etc.*) gave higher values, while the newer measurements (Paulsen,[23] Mannhart,[34] Lu,[25] Zupranska,[26] *etc.*) gave lower values. Present calculation with PEGASUS yielded a curve which is in agreement with the lower data and also with the JENDL-2 evaluation. TNG calculation gave even lower values, which however were in poor agreement in shape and value with the experimental data. One of the probable reasons for this discrepancy is poor knowledge of the level structure for the residual nucleus. In fact, levels with spin- and parity assignment are known only up to 2.98 MeV for ^{48}Sc.

For the (n, p) cross section (Fig. 5), both PEGASUS and TNG calculations gave curves simuilar in shape, *i. e.* peaked around 11.5 MeV, but these results were in disagreement with the JENDL-2 and ENDF/B-IV evalutions. It is difficult at present to say which curve represents the actual cross section, since no measurement has been done at energies except around 14 MeV.

3. Sensitivity to level density parameter and nuclear temperature

Dependence of the (n, p)-reaction cross sections on the level density parameter and nuclear temperature of the residual nucleus ^{51}Ti was analyzed. In Figs. 6 (a) and (b), the cross section values at incident neutron energies 10, 15, 20 MeV are plotted against percent change of the parameters (the "$\pm 0\%$" correspond to the adopted values $a=8.154$ MeV^{-1}, $T=1.060$ MeV, respectively). In order to see indirect influences of a change of parameters relevant to (n, p) reaction on other competing reactions, variation of the cor-

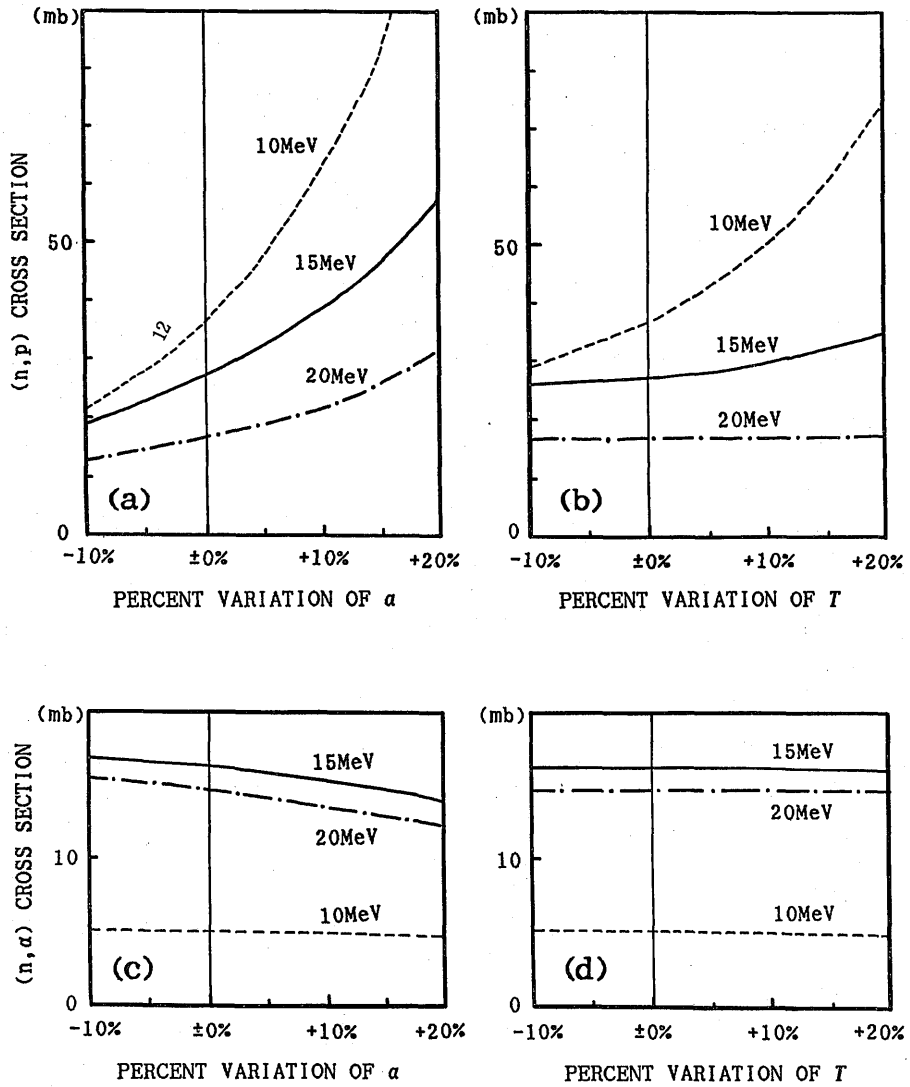

Fig. 6 Dependence of cross sections to percent variation of the level density parameter a and nuclear temperature T. (a) (n, p) cross section *vs.* a, (b) (n, p) cross section *vs.* T, (c) (n, α) cross section *vs.* a, (d) (n, α) cross section *vs.* T.

responding (n, α) cross sections are also shown in Figs. 6 (c) and (d). It can readily be seen that, in this case, (i) the (n, p) cross section is more sensitive to the level density parameter a than the nuclear temperature T, (ii) the effect is more pronounced at lower energies, and (iii) there is a reflection to (n, α) cross section though in a lesser magnitude. Possible explanation to the point (ii) lies in the fact that at higher energies the contribution of PE process becomes dominant, as can be seen in the following subsection, thus lessening the effects of the level density of the residual nucleus.

4. Effects of the PE process

The effects of variation of the Kalbach constant K on the (n, p) cross section and neutron spectrum were studied. Fig. 7 shows the (n, p) cross sections for $K=130$ MeV^3 (adopted in the present evaluation), 200 MeV^3 and ∞ (no PE effect). In the region $E_n \leqq$ 11 MeV, practically no difference was observed in the calculated cross section. In the higher energy region, smaller K-value, *i. e.* stronger PE effect, gave rise to higher cross section, thus improving the agreement with experimental data at around 14 MeV.

The energy spectrum of emitted neutrons for the case of no PE effect is also shown in Fig. 1. The high energy component above ~4.5 MeV is enhanced in the presence of PE effect, as expected. Considering that the energetic protons give rise of strong damaging effects on meterials as well as secondary proton-induced reactions, it is important that PE effect be included in nuclear data evaluations for the sake of exact estimation of these effects.

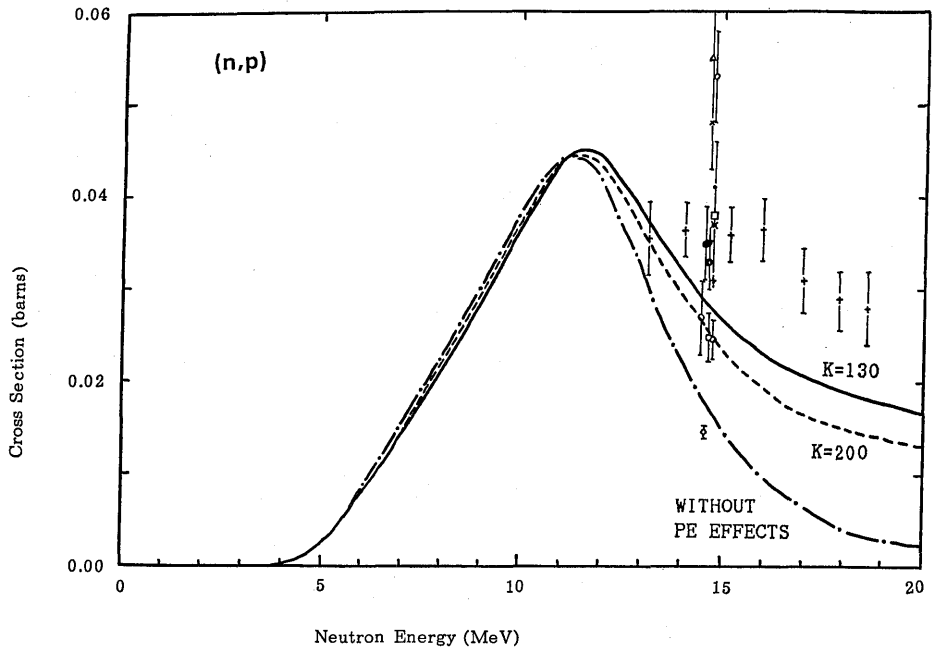

Fig. 7 Effects of different choice for the Kalbach constant K. (n, p) cross sections for $K=$ 130, 200 and ∞ MeV^3 (without PE effect) are compared.

IV. Discussion

Particle-emission reactions of ^{51}V that have large cross sections are (n, n') [473 mb at 14 MeV], (n, 2n) [486 mb] and (n, n' p) [191 mb]. As can be seen in Fig. 8, the residual nuclides of these reactions are stable ones. The (n, p) reaction [32.3 mb] leads to production of ^{51}Ti (halflife 5.76 min.) which however is not harmful from the point of view of induced activity because of its short halflife. The isotopic abundance of ^{51}V is 99.7%, the remaining 0.3% being ^{50}V. In the present work the nuclear data for ^{50}V were not evaluated, but it is known that most of the products of fast neutron-induced reac-

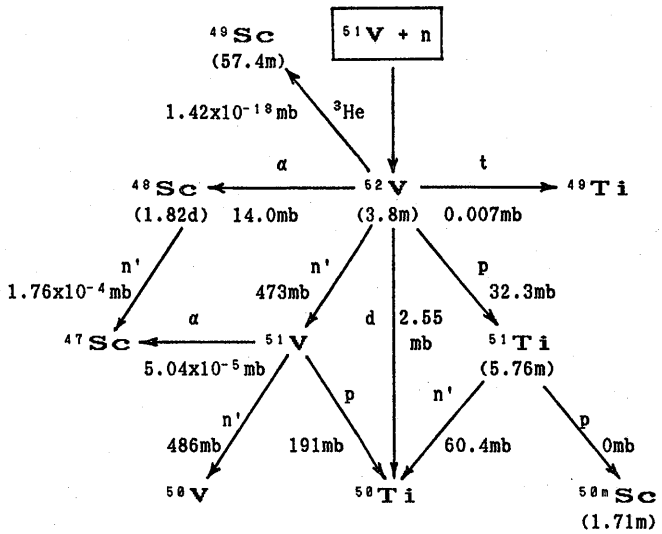

Fig. 8 Nuclear transformation and cross sections for 14-MeV neutron bombardment on ^{51}V after subsequent emission of particles. The number in parenthesis indicates the halflife.

tions of ^{50}V are stable nuclides. Therefore there are reasons to believe that vanadium is one of the hopeful materials as long as induced activity is concernd.

The simplified PE code PEGASUS was found to be a useful tool in evaluating particle-emission cross sections at least in cases where the nuclides have no strong peculiarities. In principle, of course, the full PE codes should provide more exact results, but often the level schemes for many of the reaction products, required to be input, are not well known. This may be one of the reasons for great difference between PEGASUS and TNG calculations observed in ^{51}V (n, α) ^{48}Sc cross sections because of poor knowledge of level structure for ^{48}Sc.

References

1) S. Iijima *et al.*, Private communication: see also: T. Sugi *et al.*, *Proc. of the* 1987 *Seminar on Nuclear Data*, JAERI-M 88-065 (1988) p. 486.
2) C. Y. Fu, ORNL/TM-7042 (1980); *Proc. Conf. on Nuclear Cross Sections and Technology*, Washington, 1975, vol. I, p. 328; Atomic Data and Nuclear Data Tables, **17**, 127 (1976).
3) A. Gilbert and A. G. W. Cameron, Canad. J. Phys. **24**, 63 (1965).
4) C. Kalbach, Z. Phys. **A287**, 319 (1978).
5) T. Ericson. Adv. Phys. **9**, 425 (1960).
6) C. K. Cline, Nucl. Phys. **A193**, 417 (1972).
7) A. Iwamoto and K. Harada, Pys. Rev. **C26**, 1821 (1982).
8) K. Sato, A. Iwamoto and K. Harada, Phys. Rev. **C28**, 1527 (1983).
9) A. Iwamoto and K. Harada, Nucl. Phys. **A419**, 472 (1983).
10) S. Igarasi, JAERI-1224 (1972).
11) F. C. Perey, Phys. Rev. **181**, 745 (1963).

12) J. R. Huizenga and G. Igo, Nucl. Phys. **29**, 462 (1962).
13) J. M. Lohr and W. Haerberli, Nucl. Phys. **A232**, 381 (1974).
14) F. D. Becchetti, Jr., and G. W. Greenless, *Polarization Phenomena in Nuclear Reactions* (ed. by Barshall and Haerberli), Univ. of Wisconsin Press, p. 682.
15) C. M. Lederer *et al.*, *Table of Isotopes*, John Wiley & Sons (1978).
16) D. Wilmore and P. E. Hodgson, Nucl. Phys. **55**, 673 (1964).
17) F. D. Becchetti, Jr., and G. W. Greenlees, Phys. Rev. **182**, 1190 (1969).
18) T. Nakagawa (ed.), JAERI-M 84-103 (1984).
19) J. Fréhaut, Private communication (1980).
20) I. Kumabe, J. Phys. Soc. Japan, **13**, 325 (1958).
21) M. Bormann *et al.*, J. de Phys. Radium **22**, 602 (1961).
22) J. E. Strain *et al.*, ORNL-3672 (1965).
23) A. Paulsen *et al.*, Atomkernergie **22**, 291 (1974).
24) W. Mannhart *et al.*, Z. Physik **A272**, 279 (1975).
25) H. L. Lu, Physice Energiae Fortis et Physica Nuclearis **3**, 88 (1979).
26) E. Zupranska *et al.*, Acta Physica Polonica, Section B, **11**, 853 (1980).